PAPER

Li$_2$FeSiO$_4$ nanorods bonded with graphene for high performance batteries†

Jinlong Yang,[ab] Lin Hu,[a] Jiaxin Zheng,[b] Daping He,[a] Leilei Tian,[b] Shichun Mu*[a] and Feng Pan*[b]

We synthesized a novel 2D hybrid material composed of Li$_2$FeSiO$_4$ nanorods (LFSNRs) anchored on graphene. Such a chemically bonded interface leads to electron coupling at the interface between the nano-LFS and graphene, creating effective charge transport for LFSNR@graphene hybrid cathodes. Used as a cathode material, it possesses a high capacity (300 mA h g^{-1} at 1.5–4.8 V), high charging–discharging rate (134 mA h g^{-1} @ 12 C) and long-life performance (maintaining 95% capacity over 240 cycles), which is mainly attributed to the effective depolarization introduced by the synergistic effects of LFSNRs bonded with graphene, which improves the electrochemical activity of the LFSNRs. Thus, a hybrid cathode modified with an interfacial chemical structure with nanoparticles bonded with an electrical conduction network such as graphene or CNTs can significantly enhance the electrochemical performance, and this novel type of material is very promising for commercial applications that require high energy, a long operating life, and excellent abuse tolerance, such as electric vehicles.

Introduction

Rechargeable Li-ion batteries have been widely used for consumer electronics and are desirable for the development of hybrid electric vehicles (HEV) and electric vehicles (EV), due to their high energy density and good environmental compatibility.[1] Lithium transition metal silicates, Li$_2$MSiO$_4$ (M = Fe, Mn, Co, or Ni), with high reversible capacities (the theoretical capacity reaches about 332 mA h g^{-1} for Li$_2$FeSiO$_4$ when two Li ions are intercalated), low cost, high safety, and abundant sources are very promising advanced cathode materials for next generation Li-ion batteries.[2–11] However, Li$_2$MSiO$_4$ based cathode materials inherently possess much lower ionic and electrical conductivities than those of commercial cathode materials, such as olivine-type lithium transition metal phosphates, LiMPO$_4$, and layered Li transition metal oxides, LiMO$_2$. For example, the intrinsic electronic conductivity[3] of Li$_2$FeSiO$_4$ (LFS), ∼1.0×10^{-14} S cm^{-1}, is lower than that[12] of LiFePO$_4$, 1×10^{-9} S cm^{-1}, by five orders of magnitude, and the intrinsic ionic diffusion coefficient[3] of LFS, 1.0×10^{-17} cm^2 s^{-1}, is lower than that[12] of LiFePO$_4$, 1×10^{-14} cm^2 s^{-1}, by three orders of magnitude, which seriously limits rates of Li-ion and electronic charge transport so as to influence the reversible capacity and rate performance of LFS during the insertion/extraction of two Li ions.[13,14]

In order to overcome the drawbacks of the lower ionic and electrical conductivity of the cathode materials, nanotechnologies, such as the morphology control of the nanomaterial fabrication and hybridization between the active nanomaterials and graphene or carbon nanotubes as the electron conductive network, have been widely developed to enhance the electrochemical performance of Li-ion batteries. In particular, one-dimensional (1D) nanostructures, including nanorods,[15] nanowires,[16] and nanobelts,[17] have received great interest and have been widely applied in electrode materials for Li-ion batteries, because the 1D active materials have the advantages of having short Li-ion diffusion distances, facile strain relaxation upon cycling, and very large surface to volume ratios to increase contact with the electrolyte.[18] However, pure 1D nanomaterials still suffer from poor rate performances and fast capacity fading due to their accumulation, resulting in loss of connectivity with the electron transport network during lithiation/delithiation.

Recently, graphene, with its unique two-dimensional (2D) carbon atomic crystal structure, has been widely used in hybridization with active nanomaterials for energy storage and conversion devices because of its high conductivity, light weight, high mechanical strength, structural flexibility, and large surface area.[19] Hu *et al.*[20] reported that highly conductive graphene modified LiFePO$_4$ (LFP) can assist the electron migration during cycling, diminishing the irreversible capacity at the first cycle, and leading to ∼100% coulombic efficiency without fading at various C-rates. However, the reported LFS/graphene composites[21] showed different capacities from 149 to

[a]State Key Laboratory of Advanced Technology for Materials Synthesis and Processing, Wuhan University of Technology, Wuhan 430070, China. E-mail: msc@whut.edu.cn
[b]School of Advanced Materials, Peking University Shenzhen Graduate School, Shenzhen 518055, China. E-mail: panfeng@pkusz.edu.cn

† Electronic supplementary information (ESI) available. See DOI: 10.1039/c5ta01529d

This journal is © The Royal Society of Chemistry 2015

J. Mater. Chem. A, 2015, **3**, 9601–9608 | 9601

313 mA h g^{-1}. There is no clear evidence to demonstrate the diversity of these materials. Wang *et al.*[22a] revealed that LiMn$_{0.75}$Fe$_{0.25}$PO$_4$ (LMFP) nanorods grown directly on graphene oxide over the simple physical mixture, show much better charge and discharge kinetics due to the chemical bonding between the LMFP and graphene.[22b] It can be expected that when the nano-LFS particles are anchored on graphene with a strong interaction such as chemical bonding, electron coupling at the interface between the nano-LFS and graphene will be created, with the result that the electronic transportation between the nano-LFS and graphene will significantly enhance the electrical conductivities of the hybridised nano-LFS and graphene cathode, which should possess excellent capacities and charging–discharging rates for Li-ion batteries. Herein we report a novel 2D hybrid material composed of Li$_2$FeSiO$_4$ nanorods (LFSNRs) anchored on graphene (LFSNR@graphene), which is shown to possess a high capacity of 300 mA h g^{-1}, large current charging–discharging rate and long-life performance as a cathode material. We also propose and realize the mechanism of the LFSNR@graphene with excellent electrochemical performance to modify the interfacial chemistry, with LFSNRs being chemically bonded with graphene to generate the electron coupling between the nano-LFS and graphene, which makes the LFSNRs feel direct electric-potential without IR (current-resistant) deduction to create the depolarization effect to enhance the electrochemical activity of the LFSNRs.

Experimental

Synthesis of LFSNRs and LFSNR@graphene hybrid

The free Li$_2$FeSiO$_4$ nanorods (LFSNRs) were synthesized *via* a hydrothermal method. First, 0.01 mol of Fe(NO$_3$)$_3$·9H$_2$O was thoroughly dissolved in 10 mL of ethylene glycol with 0.01 mol of ascorbic acid until the crimson colour faded; second, 0.01 mol of tetraethyl orthosilicate (TEOS) and 0.04 mol of LiOH·2H$_2$O were added into 50 mL of deionized water with vigorous stirring for 40 min; third, the two solutions were rapidly mixed to obtain a dark green colloidal solution, which was transferred into a 100 mL Teon-lined stainless steel autoclave and maintained at 200 °C for 6 days. The grayish LFSNR precipitate was collected, washed with water and ethanol several times, and dried at 80 °C in vacuum for 12 h. To prepare the LFSNR@graphene hybrid material, we used a simple PVP anchoring technology. First, 0.3 g of LFSNR powder was added to 30 mL of a homogeneous aqueous solution containing 0.03 g of PVP and 0.03 g of graphene oxide nanosheets prepared by a modified Hummers' method (see the ESI† for more info.). The mixture was vigorously stirred for 30 minutes, subsequently freeze-dried and mildly heated at 600 °C for 6 h under an Ar atmosphere.

Material characterization

X-ray diffraction (XRD) data of the samples were collected with a D$_8$ Advance X-ray diffractometer, using Cu K$_\alpha$ radiation ($\lambda = 1.5418$ Å) in a 2θ range from 10° to 80° at room temperature. Microstructures were observed by Field-emission scanning electron microscopy (FESEM) (Hitachi S-4800, 10 kV), and transmission electron microscopy (TEM) and high-resolution transmission electron microscopy (HRTEM) (JEM-2100F). Raman spectra were obtained using an RM-1000 Renishaw confocal Raman microspectroscope with 514.5 nm laser radiation at a laser power of 0.04 mW in the range 200–3000 cm^{-1}. The valence state of the key elements in the samples was studied by X-ray photoelectron spectroscopy (XPS) (PHI Quantera, U-P).

Electrochemical measurements

The electrochemical properties of the materials were tested with 2032-type coin cells assembled in a glove box filled with pure argon. A lithium pellet was used as the anode, Celgard 2400 as the separator and a 1.0 M solution of LiPF$_6$ in ethylene carbonate/dimethyl carbonate (1/1 v/v) (bought from Zhangjiagang Guotai-Huarong New Chemical Materials Co., Ltd. China) as the electrolyte, and the cathode electrodes were produced with 75% active material, 15% conducting agent (Vulcan XC-72) and 10% poly-(tetrafluoroethylene) (PTFE) binder. Galvanostatic charge–discharge measurements were performed using a multichannel battery testing system (LAND CT2001A). All the measurements were carried out at a room temperature of 30 ± 5 °C. Charge–discharge specific capacities mentioned in this paper were calculated using the mass of LFS determined by excluding the carbon content and capacity of graphene.

Results and discussion

The synthesis route for LFSNR@graphene is illustrated in Fig. 1. First, LFSNR was obtained *via* a hydrothermal method using a suspension with a 4 : 1 : 1 : 0.5 molar ratio of LiOH, TEOS (ethyl orthosilicate), Fe(NO$_3$)$_3$·9H$_2$O and ascorbic acid (AA) in a 5 : 1 volume ratio of water/ethylene glycol (EG) at 200 °C for 6 days. AA & EG were not only used as the reducing agent but also as the solvent, possessing a good coordinating ability and playing a critical role in the connection of the precursors and ligand to form coordination complexes with iron ions. This promotes the preferred orientation of the crystals to be grown as nanorods. Subsequently, the prepared LFSNRs were anchored on graphene oxide nanosheets. After freeze drying, 2D hybrid materials with Li$_2$FeSiO$_4$ nanorods anchored on graphene oxide nanosheets were formed and further heated at 600 °C for 6 h to obtain the LFSNR@graphene hybrid materials. This process is also described in the "Synthesis of graphene oxide nanosheets" (ESI) with SEM images (Fig. S1†).
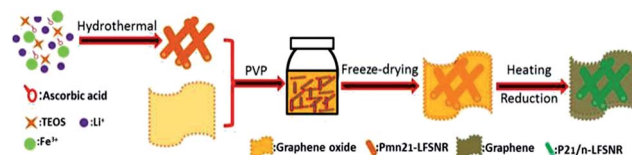

Fig. 1 Schematic illustration of the synthesis of the LFSNR@graphene hybrids.

Typical XRD patterns of the free-standing LFSNRs and LFSNR@graphene are shown in Fig. 2a. The distinguishable sharp intense peaks correspond to the highly crystalline nature of the as-prepared LFS. As reported, there are at least three different structures for LFS, namely a monoclinic structure with space group $P2_1/n$,[14] and two orthorhombic structures with space groups $Pmn2_1$ (ref. 22) and $Pmnb$.[23] The diffraction peaks of the LFSNRs were indexed according to the orthorhombic $Pmn2_1$ structure with the lattice parameters: $a = 0.628$ nm, $b = 0.533$ nm and $c = 0.497$ nm, and a few Fe_3O_4 impurities were unavoidably present in the samples. Different from the $Pmn2_1$ structure, LFSNR@graphene has a monoclinic $P2_1/n$ structure with cell parameters of $a_s = 0.824$ nm, $b_s = 0.502$ nm and $c_s = 0.825$ nm and $\beta_s = 99.09°$ confirmed by a superstructure peak at $32°$. In addition, the broad peak at approximately $22°$ corresponds to graphene. Fig. 2b shows a schematic of the $Pmn2_1$ and $P2_1/n$ phases of LFS. All LiO_4, FeO_4 and SiO_4 tetrahedra are connected by corner-sharing and point in the same direction parallel to the c-axis for the $Pmn2_1$ phase. When the LFSNRs were heated at 600 °C, half of the LiO_4, FeO_4, and SiO_4 tetrahedra turned to point in the opposite direction, parallel to the b_s-axis, to become the $P2_1/n$ phase. A similar LFS phase change after heating was also reported by Yabuuchi et al.[24] Meanwhile, first-principle investigations of Li ion diffusion[25] have shown that there are two diffusion channels for Li ions in the $P2_1/n$-LFS structure, but only one diffusion channel along the b_s-axis is left when Li_2FeSiO_4 is delithiated to become $LiFeSiO_4$.

The SEM and TEM images (Fig. 2c) reveal the hydrothermal products retain a 1D nanocrystal morphology, with features similar to nanorod with a length of 200–300 nm and diameter of 10–25 nm. The HRTEM image (inset of Fig. 2c) shows a lattice spacing of $d = 0.53$ nm, corresponding to the (010) plane of $Pmn2_1$-LFS crystals. The fast Fourier transform pattern of the lattice structure exhibits a selected zone of single-crystalline LFS ($Pmn2_1$), which can be identified as the [001] projection of the reciprocal lattices, implying that the long axes of the nanorods are along the a-axis of the LFS crystals. The enlarged HRTEM image shows that the obtained distances of the different atomic dots correspond to the distances of the central atoms in the LiO_4, FeO_4, and SiO_4 tetrahedra of the exposed (001) facets (inset of Fig. 2c), indicating a perfect crystal obtained under these conditions. Fig. 2d shows the SEM and TEM images of the LFSNR@graphene. It can be seen that the LFSNR@graphene hybrid is formed as a 2D nanosheet with nanorods firmly embedded in the graphene sheets (inset of Fig. 2d). Note that the nanorods maintain good crystallinity (Fig. 2a) after the
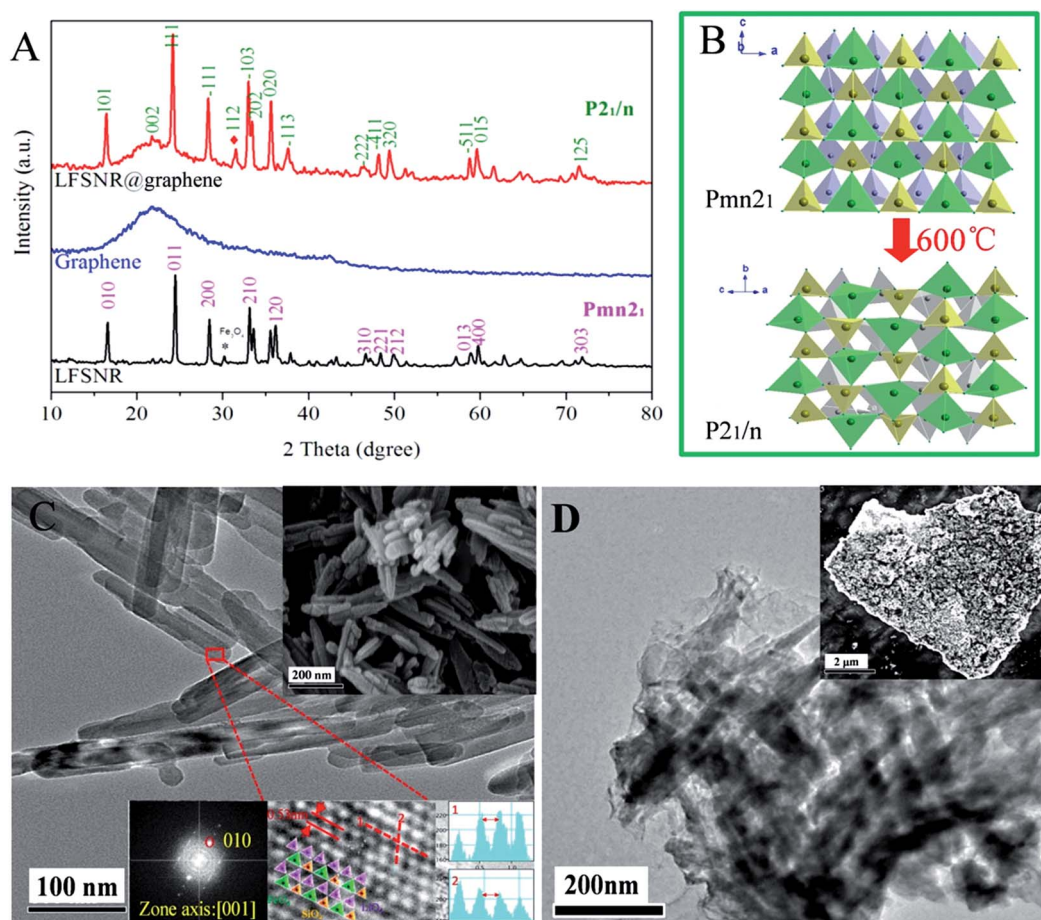

Fig. 2 Characterization of the LFSNR@graphene hybrids: (a) XRD patterns (b) schematic illustration of the structural change from the $Pmn2_1$ to the $P2_1/n$ phase for LFS, (c) SEM and TEM images of the free LFSNRs; (d) SEM and TEM images of the LFSNR@graphene hybrids.

This journal is © The Royal Society of Chemistry 2015

J. Mater. Chem. A, 2015, **3**, 9601–9608 | **9603**

phase change occurs from $Pmn2_1$-LFS to a $P2_1/n$-LFS structure after heating.

In order to find out whether chemical bonding exists at the interface between the nano-LFS particles and graphene, various cross-checking experiments were carried out using TEM, Raman spectroscopy, and X-ray photoelectron spectroscopy (XPS), as shown in Fig. 3. The TEM image shown in Fig. 3a shows the LFS nanorod, graphene nanosheet, and the interface around the LFS anchored on graphene. The TEM image shown in Fig. 3b shows that the interplanar distance, 0.53 nm, is related to the (101) plane of $P2_1/n$-LFS, the long axes of the nanorods (the crystal growth direction) are perpendicular to the <101> direction, and the short axes are parallel to the graphene sheet along the b-axis, which is one of the Li$^+$ diffusion directions in the $P2_1/n$-LFS crystals.[25] The high-resolution TEM images (Fig. 3a and b) show that the interface layer around the LFS anchored on graphene includes two parts: one is the free-standing graphene layer structure with defects, the other is the region in contact with the LFS crystal, where the discrete layers are shown in the "interface" zone in Fig. 2b, indicating the LFS crystal has transformed into amorphous LFS. Thus, it can be proposed that the new layers at the interface around the LFS anchored on graphene are generated by a type of chemical bonding interaction between the LFS and graphene.

Raman spectra of the LFSNR, graphene and LFSNR@graphene materials are shown in Fig. 3c. For comparison, the samples of graphene and the LFSNRs ($P2_1/n$) were obtained using the same graphene oxide nanosheets (GONS) and LFSNRs ($Pmn2_1$) by the same heating treatment at 600 °C for 6 h as that used to prepare the LFSNR@graphene. For the LFSNRs, several peaks in the range 400–700 cm^{-1} correspond to Fe–O vibrations,[10] and the peak at ~800 cm^{-1} is assigned to the symmetric stretching internal vibration modes of the SiO$_4$ anions in LFS.[10] Raman spectra of both graphene and LFSNR@graphene show a strong and sharp peak at around 1590 cm^{-1} (G band), which is assigned to the E_{2g} stretching vibration of sp^2 carbon bonds. The other at around 1335 cm^{-1} (D band) is due to the activation of an otherwise symmetry forbidden set of modes by the defects in the sp^2 electronic network. In addition, the existence of a characteristic peak at ~2700 cm^{-1} (2D band) indicates that the LFSNR@graphene hybrids possess graphitic structures, which can improve the electronic conductivity of the cathode material. The ratio of the D to G band intensity (I_D/I_G) is widely used to evaluate the degree of ordering in the carbon materials.[26] Meanwhile, the exact positions of the bands depend on the laser frequency and the details of the electronic and phonon energy dispersion.[27] A closer look at the spectrum indicates that the bands are shifted by ~5 cm^{-1} to lower frequencies (red-shift)[22a] in the LFSNR@graphene hybrids compared to pristine graphene, suggesting that the shift is related to surface interactive effects. The I_D/I_G ratio of the LFSNR@graphene hybrid is 1.26, which is higher than the value of 1.17 for graphene, indicating that there are more defects on graphene generated at the interface. Both the Raman red-shift and the I_D/I_G ratio increase for LFSNR@graphene can be realized as the degradation of the sp^2 electronic network of graphene due to the creation of the C atom sp^3 hybrid at the interface of the LFSNR and the graphene, such as the (graphene)–C–O–Fe– bonding shown in Fig. 3e.

Strong evidence for the interfacial chemical bonding between the LFSNRs and graphene can be observed through XPS by comparing the samples of the LFSNR@graphene with the pure graphene (Fig. 3d). The scale of the binding energy (B.E.) in the XPS spectrum is referenced by setting the B.E. of C 1s to 284.6 eV. The observed C 1s BEs of LFSNR@graphene are 285.6 eV (C–O), 287.5 eV (C=O) and 289.5 eV (C=O–O), respectively. The high atomic percentages (52.12%) of C=C further indicates that the hybrid possesses graphene composition which results in superior conductivity. Compared to the graphene reduced by the same graphene oxide, extra oxygen-containing functional groups (C–O, C=O–O) are present in the LFSNR@graphene. It can be proposed that the interface structure with –C–O–Fe, –C–O–Li and –C–O–Si chemical bonding is generated during the heat treatment at 600 °C, while the graphene oxide with free C–O and C=O–O groups is reduced to graphene under the same heat treatment conditions. As a result, a homogenous 3D conductive network is connected to the LFS crystal. In addition, the Fe 2p$^{2/3}$ B.E. of 711.8 eV (Fig. S2,† right) is consistent with the B.E. of Fe^{2+}.[5] The Si 2p B.E. of 101.8 eV (Fig. S2,† left) is in line with that of Si^{4+} in polysiloxane, indicating the formation of an orthosilicate [SiO$_4$] structure.[5] Hence, the interfacial chemical structure can be
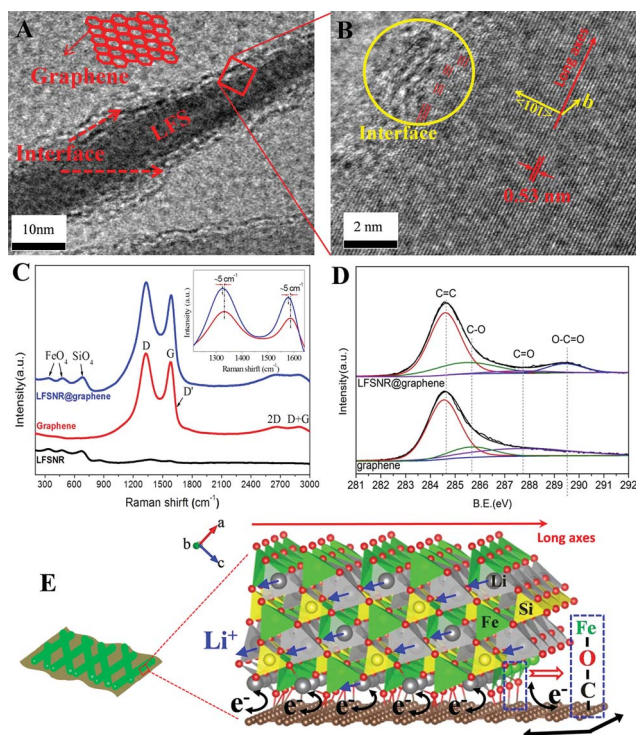

Fig. 3 Bond effects of the LFSNRs and graphene: (a) TEM image of a single nanorod in the hybrid material, (b) HRTEM image of a single nanorod in the hybrid material, (c) Raman spectra of free LFSNRs, graphene and the LFSNR@graphene hybrid, (d) binding energy at the C 1s region for graphene and the LFSNR@graphene hybrid, (e) electron and Li ion transport schematic of the Li$_2$FeSiO$_4$ nanorods bonded with graphene.

9604 | J. Mater. Chem. A, 2015, **3**, 9601–9608

This journal is © The Royal Society of Chemistry 2015

Paper

realized as the C–O and C=O–O groups of the graphene oxide nanosheets chemically bond with the unsaturated surface Li, Si and Fe atoms of the LiO_4, SiO_4 and FeO_4 tetrahedra. As a result, the symmetries of the LiO_4, SiO_4 and FeO_4 tetrahedra on the surface of the LFSNRs are offset as shown in Fig. 3e.

Such a chemically bonded interface of LFSNR@graphene would lead to easier charge transfer than that resulting from physical van der Waals interaction. In addition, in the homogenous 3D conductive network, this combined effect will improve the electron transport of LFSNR@graphene, enhancing the electrical conductance greatly. A comparative investigation of the electrochemical performance of the free LFSNRs and the LFSNR@graphene hybrids as cathodes for Li-ion batteries was carried out as described below. Coin cells with metallic lithium as the anode were assembled to investigate the electrochemical performance of these cathodes. Firstly, the as-prepared batteries were cycled between 1.5 and 4.8 V with a high voltage electrolyte at a room temperature of 30 ± 5 °C and current density of 20 mA g^{-1}, and the CV curves in Fig. S3† support the reliability of the high-quality commercial electrolytes. Furthermore, as noted, the capacity of graphene is ~200 mA h g^{-1} (Fig. S5†). According to graphene content of ~4.7 wt% (Fig. S4†), ~9.4 mA h g^{-1} was excluded when the specific capacities were calculated. In order to demonstrate the possible structural advantages of the hybrids, the free-standing LFSNRs (graphene as conductive additives) were used as contrast. Fig. S6† shows the typical charge–discharge curves of the LFSNRs at 20 mA g^{-1} between 1.5 and 4.8 V for 10 cycles. Note that the initial cycle shows a high irreversible capacity. Subsequently, for the 2nd cycle, it possesses a discharge specific capacity of 165.2 mA h g^{-1} with a high coulombic efficiency of 99%, representing a reversible extraction of one Li ion per formula unit. However, a large charge–discharge platform voltage difference indicates large polarization impedance, and the low specific capacity is because of its electrochemically inactive nature.[5] Compared with our previously reported micro-sized LFS hierarchical shuttle,[28] the nano-sized LFS rods show a relatively poor cycle performance, which could be due to the aggregation of the nanomaterials that hinder the transfer of Li ions under cycled processes. However, the electrochemical performance was greatly improved after anchoring LFSNRs on graphene. The 10 cycle charge–discharge curves of the LFSNR@graphene hybrid at a current density of 20 mA g^{-1} are shown in Fig. 4. Compared to the LFSNRs, the hybrid presents a significantly increased discharge specific capacity from 165.2 to 306.4 mA h g^{-1} (approaching the theoretical capacity of 332 mA h g^{-1}) with two Li ion storages per LFS formula unit. After 20 cycles, the discharge capacity finally stabilises at 284 mA h g^{-1}, corresponding to a capacity retention rate of 94%. The overpotential was evaluated from the difference between the charge potential and discharge potential at the half reversible capacity, noted as $\Delta V(Q/2)$.[29] The overpotential of LFSNR@graphene (0.41 V) is much lower than that of free the LFSNRs (0.77 V). The electrochemical impedance spectra (EIS) were used to provide further insights (Fig. 5). The Nyquist plots indicate that the charge transfer resistance (R_{ct}) of the LFSNR@graphene cathode is 70 Ω, much lower than the 240 Ω of the LFSNR, indicating higher

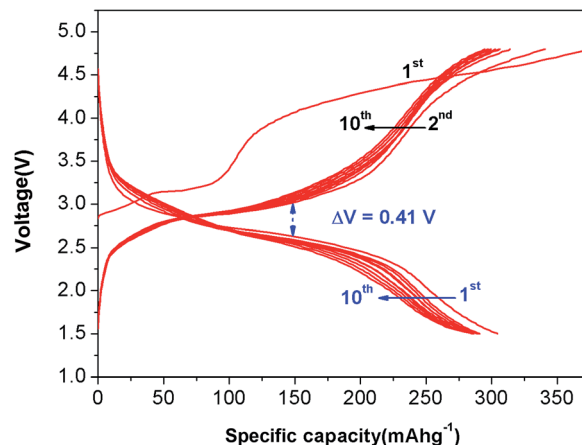Fig. 4 Typical galvanostatic charge–discharge curves of the LFSNRs bonded with graphene at 20 mA g^{-1} in the range 1.5–4.8 V.

electrochemical activity of LFSNR@graphene than that of LFSNR. Moreover, after ten cycles, the R_{ct} values of LFSNR@graphene and LFSNRs increase to 78 Ω and 310 Ω, respectively. The above results demonstrate the better structure stability and cyclability of the LFSNR@graphene than the free LFSNRs, and suggest that LFSNR@graphene has the faster kinetics for Li ion insertion/extraction.

To evaluate the advantages of the LFSNR@graphene hybrid structure, the rate performance at progressively larger current densities was measured, ranging from 0.05 to 2 A g^{-1} (Fig. 6a). Firstly, note that the free LFSNR cathode shows a low discharge capacity of less than 20 mA h g^{-1} at a high density of 2 A g^{-1} (12 C). For the LFSNR@graphene hybrid, discharge specific capacities of 280, 249, 209, 176 and 134 mA h g^{-1} can be reached at current densities of 0.05 (0.3 C), 0.1 (0.6 C), 0.2 (1.2 C), 1 (6 C) and 2 A g^{-1} (12 C), respectively, which are higher than those of most of the other previously reported LFS cathodes, including 3D macroporous graphene-based Li_2FeSiO_4 composites[30] (excluding the capacity of graphene) (Fig. S7†). Even when

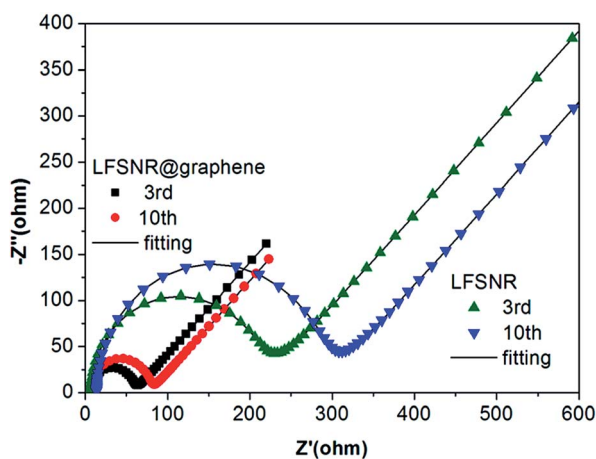Fig. 5 AC impedance plots of the free LFSNRs and LFSNRs bonded with graphene cathodes, from 0.01 Hz to 100 kHz.
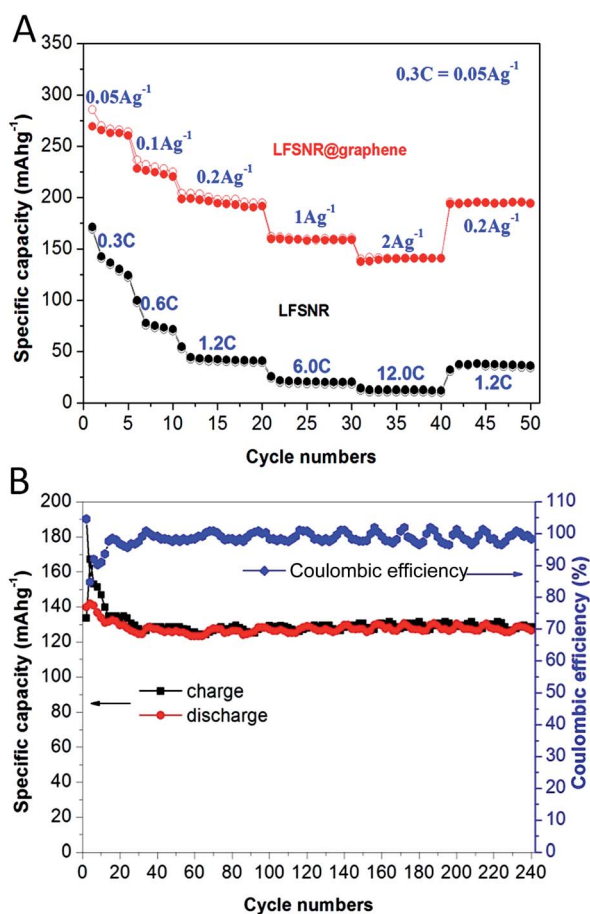
Fig. 6 Electrochemical measurements of the LFSNR@graphene hybrid and free LFSNR cathodes: (a) specific capacitance variation at different current densities, (b) cycle capacity at a high rate current density of 2 A g^{-1} for 240 cycles.

Fig. 7 Cyclic voltammetry (CV) of the LFSNRs bonded with the graphene hybrid compared to the free LFSNR cathode.

suffering from a rapid change in the current density, the electrode exhibits a stable capacity at each value. When the current was turned back to 0.2 A g^{-1}, the full (100%) capacity recovered and was maintained for the following 10 cycles without an obvious decrease, indicating excellent robustness. Significantly, the 2D LFSNR@graphene hybrid cathode also demonstrated long-life performance at a high current density. Fig. 6b reveals the discharge specific capacity of 134 mA h g^{-1} without any loss at 2 A g^{-1} for 240 cycles except for the initial few cycles, and the coulombic efficiency is ~100%, indicating a super high stability and a very promising application scenario in cathode materials for high power Li-ion batteries.

Cyclic voltammetry (CV) was conducted to reveal the electrochemical reactions of the LFSNR@graphene hybrid (Fig. 7). For the free LFSNRs, only one pair of redox peaks was observed at 3.2/2.5 V, corresponding to the redox reaction[2,3] of Fe^{2+}/Fe^{3+}, whereas multiple pairs of redox peaks were recorded for the LFSNR@graphene hybrid. The redox reaction of the Fe^{2+}/Fe^{3+} is down-shifted by about 0.2 V (located at 3.0/2.6 V), indicating the low overpotential due to the depolarization with high electronic conductivity of the LFSNR@graphene hybrid as cathodes. Significantly, two reversible anodic peaks appear at about 4.3
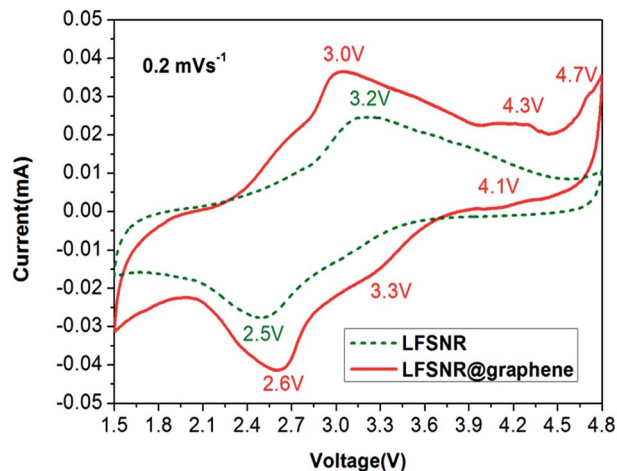
and 4.7 V, and the corresponding cathodic peaks are centered at 3.3 and 4.1 V, respectively, indicating some novel electrochemical reactions to increase the lithium storage in the cathode. Therefore, all of this corresponds to a depolarization effect,[31] which is introduced by the synergistic effects of the LFSNRs chemically bonding on graphene and the greatly improved electrical conductance.

Different rate cyclic voltammetry measurements from 0.1 to 0.5 mV s^{-1} were used to characterize the kinetics of the LFSNR@graphene hybrid material (Fig. S8†). Assuming that the current obeys a power-law relationship with the sweep rate leads to:[32,33]

$$i_P = a\nu^b$$

where a and b are adjustable values. Whereas a b-value of 0.5 would indicate that the current is controlled by a semi-infinite linear diffusion, the value of 1 indicates that the current is surface-controlled. Fig. 8 shows the b-values (which are obtained from the slope of a plot of the peak current versus the potential scan rate on a logarithmic scale (Fig. S9†)) at different anodic and cathodic peak positions. The b-values at 2.6 (anodic), 3.0 (anodic), 3.3 (anodic), 4.3 (anodic) and 4.7 V (anodic) are between 0.5 and 1, indicating a concurrence of both lithium semi-infinite linear diffusion of the LFNR crystal and the surface reaction of graphene. The redox reaction corresponding to the peaks at 4.3 and 4.7 V are similar to current reported redox[10,11] of Fe^{3+}/Fe^{4+}, which has been carried out using ex situ Mössbauer spectroscopy[9] and in situ XANES spectroscopy.[7] In addition, it was also found that the b-value below 1.6 V was 0.98 (approaching 1) and was independent of the charge–discharge rate, indicating a full surface reaction of graphene and the LFS-nanorods.

Further investigation of the charge–discharge curves were used to understand the excellent electrochemical performance of the LFSNR@graphene hybrid material. Fig. 9a is a discharge curve at a current density of 20 mA g^{-1}. It can be observed that there are three parts contributing to the total

9606 | J. Mater. Chem. A, 2015, 3, 9601–9608

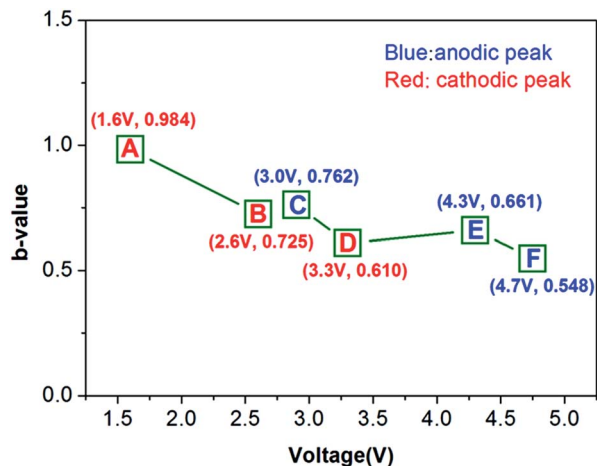This journal is © The Royal Society of Chemistry 2015

Fig. 8   b-values obtained from the slope of the peak current *versus* the CV scan rate on a logarithmic scale (Fig. S6†) at different anodic and cathodic peak positions.
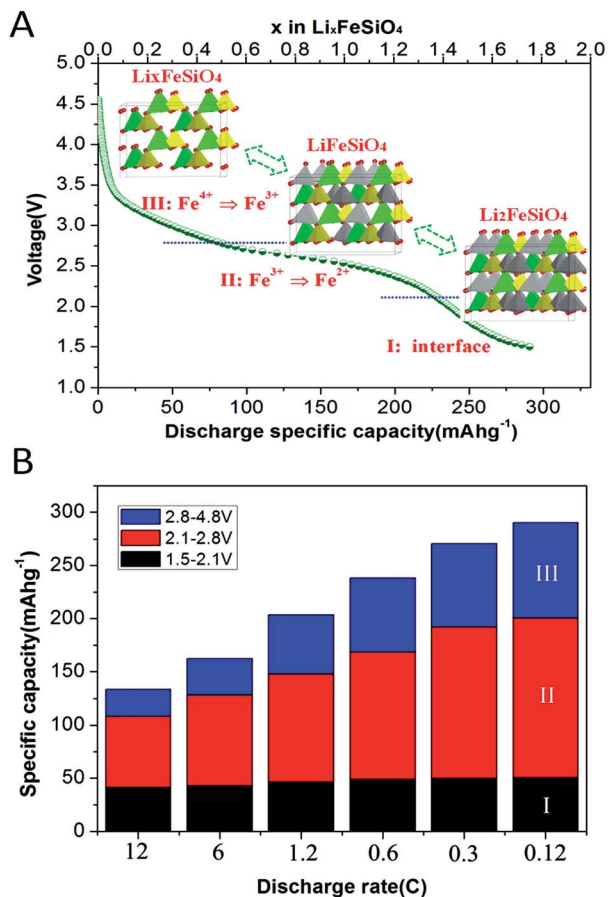

Fig. 9   (a) A discharge curve of the LFSNR@graphene hybrid at a current density of 20 mA g^{-1}, the inset shows a schematic illustration of the LFSNR@graphene hybrid for Li storage; (b) variation of the capacity in different regions *versus* the discharge rate for the LFSNR@graphene hybrid.

discharge capacity. The first is the sluggish slope capacity (region I) between 1.5 and 2.1 V. Fig. 9b shows the variation of capacity in different regions *versus* the discharge rate (the different charge–discharge curves at different current rates from Fig. S10†), in which the capacity for region I is almost constant (40 mA h g^{-1}), further verifying that the favored lithium storage process is not a kinetic phenomenon. Therefore, we speculate that region I corresponds to an interfacial Li storage procession of the LFSNRs and graphene, which is similar to that reported for LFP-NP@NPCM[34] (LiFePO$_4$ nanopaticles embedded in a nanoporous carbon matrix) at low potential. The second is the capacity plateau (region II) at 2.6 V corresponding to the reduction reaction of Fe^{3+} to Fe^{2+}, with an increase in current rate from 0.12 to 12 C, the discharge capacity decreased from 154 to 84 mA h g^{-1}, accounting for 65% of the total capacity. Note that the capacity, 154 mA h g^{-1} at 2.6 V @ 0.12 C, is quite close to half lithium insertion to Li$_2$FeSiO$_4$ with the reduction reaction of Fe^{3+} to Fe^{2+}. The third is region III between 2.8 and 4.8 V, corresponding to the reduction reaction of Fe^{4+} to Fe^{3+}, with the increase of current rate, the discharge capacity toboggans.

Conclusions

In summary, we synthesized single crystalline LFS nanorods, and subsequently bonded them with highly conducting graphene nanosheets by a simple PVP modified route. Such a chemically bonded interface leads to electron coupling at the interface between the nano-LFS and graphene to create effective charge transport for LFSNR@graphene hybrid cathodes. Used as a cathode material, it possesses a high capacity (~300 mA h g^{-1} at 1.5–4.8 V), high charging–discharging rate (134 mA h g^{-1} @ 12 C) and long-life performance (maintaining 95% capacity over 240 cycles), which is mainly attributed to the effective depolarization introduced by the synergistic effects of the LFSNRs bonded with graphene, which improves the electrochemical activity of the LFSNRs. Thus, a hybrid cathode modified with an interfacial chemical structure with nanoparticles bonded with an electrical conduction network such as graphene or CNTs can significantly enhance the electrochemical performance, and this novel type of material is very promising for commercial applications that require high energy, long operating lives, and excellent abuse tolerance, such as electric vehicles.

Acknowledgements

Notes and references

1 (a) J. M. Tarascon and M. Armand, *Nature*, 2001, **414**, 359; (b) K. Kang, Y. S. Meng, J. Bréger, C. P. Grey and G. Ceder, *Science*, 2006, **311**, 977; (c) X. Xiao, P. Lu and D. Ahn, *Adv. Mater.*, 2011, **23**, 3911; (d) J. Hassoun and B. Scrosati, *Adv. Mater.*, 2010, **22**, 5198; (e) B. Scrosati, J. Hassoun and Y. K. Sun, *Energy Environ. Sci.*, 2011, **4**, 32875; (f) G. Jeong, Y. U. Kim, H. Kim, Y. J. Kim and H. J. Sohn, *Energy Environ. Sci.*, 2011, **4**, 1986.

2 (a) A. Nytén, A. Abouimrane, M. Armand, T. Gustafsson and J. O. Thomas, *Electrochem. Commun.*, 2005, **7**, 156; (b) A. Nytén, M. Stjerndahl, H. Rensmo, H. Siegbahn, M. Armand, T. Gustafsson and J. O. Thomas, *J. Mater. Chem.*, 2006, **16**, 3483; (c) A. Nytén, S. Kamali, L. Häggström, T. Gustafsson and J. O. Thomas, *J. Mater. Chem.*, 2006, **16**, 2266.

3 (a) R. Dominko, *J. Power Sources*, 2006, **184**, 462; (b) R. B. Araujo, R. H. Scheicher, J. S. de Almeida, A. Ferreira da Silva and R. Ahuja, *Solid State Ionics*, 2013, 247.

4 Z. Gong and Y. Yang, *Energy Environ. Sci.*, 2011, **4**, 3223.

5 D. Rangappa, K. D. Murukanahally, T. Tomai, A. Unemoto and I. Honma, *Nano Lett.*, 2012, **12**, 1146.

6 Y. Zhao, J. Li, N. Wang, C. Wu, Y. Ding and L. Guan, *J. Mater. Chem.*, 2012, **22**, 18797.

7 D. Lv, J. Bai, P. Zhang, S. Wu, Y. Li, W. Wen and Y. Yang, *Chem. Mater.*, 2013, **25**, 2014.

8 T. Muraliganth, K. R. Stroukoff and A. Manthiram, *Chem. Mater.*, 2010, **22**, 5754.

9 (a) D. Lv, W. Wen, X. Huang, J. Bai, J. Mi, S. Wu and Y. Yang, *J. Mater. Chem.*, 2011, **21**, 9506; (b) J. Yang, X. Kang, L. Hu, X. Gong and S. Mu, *J. Mater. Chem. A*, 2014, **2**, 6870.

10 Z. Chen, S. Qiu, Y. Cao, J. Qian, X. Ai, K. Xie and H. Yang, *J. Mater. Chem. A*, 2013, **1**, 4988.

11 J. Bai, Z. Gong, D. Lv, Y. Li, H. Zou and Y. Yang, *J. Mater. Chem.*, 2012, **22**, 12128.

12 (a) S. Y. Chung, J. T. Bloking and Y. M. Chiang, *Nat. Mater.*, 2002, **1**, 123; (b) C. Ouyang, S. Shi, Z. Wang, X. Huang and L. Chen, *Phys. Rev. B: Condens. Matter Mater. Phys.*, 2004, **69**, 104303.

13 A. Liivat and J. O. Thomas, *Solid State Ionics*, 2011, **192**, 58.

14 S. I. Nishimura, S. Hayase, R. Kanno, M. Yashima, N. Nakayama and A. Yamada, *J. Am. Chem. Soc.*, 2008, **130**, 13212.

15 A. M. Cao, J. S. Hu, H. P. Liang and L. J. Wan, *Angew. Chem., Int. Ed.*, 2005, **44**, 4391.

16 L. F. Cui, Y. Yang, C. M. Shu and Y. Cui, *Nano Lett.*, 2009, **9**, 3370.

17 L. Q. Mai, B. Hu, W. Chen, Y. Y. Qi, C. S. Lao, R. S. Yang and Z. L. Wang, *Adv. Mater.*, 2007, **19**, 3712.

18 (a) C. Han, Y. Pi, Q. An, L. Mai, J. Xie, X. Xu and X. He, *Nano Lett.*, 2012, **12**, 4668; (b) M. Yan, F. Wang, C. Han, X. Ma, X. Xu, Q. An and L. Mai, *J. Am. Chem. Soc.*, 2013, **135**, 18176; (c) X. Xu, Y. Z. Luo, L. Q. Mai, Y. L. Zhao, Q. Y. An, L. Xu and Q. J. Zhang, *NPG Asia Mater.*, 2012, **4**, e20.

19 (a) C. Lee, X. Wei, J. W. Kysar and J. Hone, *Science*, 2008, **321**, 385; (b) F. Liu, P. Ming and J. Li, *Phys. Rev. B: Condens. Matter Mater. Phys.*, 2007, **76**, 064120; (c) S. Bae, H. Kim, Y. Lee, X. Xu, J. S. Park, Y. Zheng and S. Iijima, *Nat. Nanotechnol.*, 2010, **5**, 574; (d) A. S. Mayorov, R. V. Gorbachev, S. V. Morozov, L. Britnell, R. Jalil, L. A. Ponomarenko, P. Blake, K. S. Novoselov, K. Watanabe, T. Taniguchi and A. K. Geim, *Nano Lett.*, 2011, **11**, 2396; (e) S. V. Morozov, K. S. Novoselov, M. I. Katsnelson, F. Schedin, D. C. Elias, J. A. Jaszczak and A. K. Geim, *Phys. Rev. Lett.*, 2008, **100**, 016602; (f) A. A. Balandin, *Nat. Mater.*, 2011, **10**, 569; (g) Y. Zhu, S. Murali, M. D. Stoller, K. J. Ganesh, W. Cai, P. J. Ferreira and R. S. Ruoff, *Science*, 2011, **332**, 1537.

20 L. H. Hu, F. Y. Wu, C. T. Lin, A. N. Khlobystov and L. J. Li, *Nat. Commun.*, 2013, **4**, 1687.

21 (a) H. Zhu, X. Wu, L. Zan and Y. Zhang, *Electrochim. Acta*, 2014, **117**, 34; (b) H. Zhu, X. Wu, L. Zan and Y. Zhang, *ACS Appl. Mater. Interfaces*, 2014, **6**, 11724; (c) D. Bhuvaneswari and N. Kalaiselvi, *Dalton Trans.*, 2014, **43**, 18097; (d) L. L. Zhang, S. Duan, X. L. Yang, G. Peng, G. Liang, Y. H. Huang, Y. Jiang, S. Ni and M. Li, *ACS Appl. Mater. Interfaces*, 2013, **5**, 12304.

22 (a) H. Wang, Y. Yang, Y. Liang, L. F. Cui, H. Sanchez Casalongue, Y. Li, G. Hong, Y. Cui and H. Dai, *Angew. Chem.*, 2011, **123**, 7502; (b) G. Mali, C. Sirisopanaporn, C. Masquelier, D. Hanzel and R. Dominko, *Chem. Mater.*, 2011, **23**, 2735.

23 C. Sirisopanaporn, A. Boulineau, D. Hanzel, R. Dominko, B. Budic, A. R. Armstrong and C. Masquelier, *Inorg. Chem.*, 2010, **49**, 7446.

24 N. Yabuuchi, Y. Yamakawa, K. Yoshii and S. Komaba, *Dalton Trans.*, 2011, **40**, 1846.

25 R. B. Araujo, R. H. Scheicher, J. S. de Almeida, A. Ferreira da Silva and R. Ahuja, *Solid State Ionics*, 2013, **247**, 8.

26 (a) X. Zhou, F. Wang, Y. Zhu and Z. Liu, *J. Mater. Chem.*, 2011, **10**, 3353; (b) S. C. Mu, H. L. Tang, S. H. Qian, M. Pan and R. Z. Yuan, *Carbon*, 2006, **44**, 762.

27 T. Muraliganth, A. V. Murugan and A. Manthiram, *J. Mater. Chem.*, 2008, **8**, 5661.

28 J. Yang, X. Kang, D. He, T. Peng, L. Hu and S. Mu, *J. Power Sources*, 2013, **242**, 171.

29 L. Mai, Q. Wei, Q. An, X. Tian, Y. Zhao, X. Xu and Q. Zhang, *Adv. Mater.*, 2013, **25**, 2969.

30 H. Zhu, X. Wu, L. Zan and Y. Zhang, *ACS Appl. Mater. Interfaces*, 2014, **6**, 11724.

31 Z. Wu, X. Han, J. Zheng, Y. Wei, R. Qiao, F. Shen, J. Dai, L. Hu, K. Xu, Y. Lin, W. Yang and F. Pan, *Nano Lett.*, 2014, **14**, 4700.

32 J. Come, P. L. Taberna, S. Hamelet, C. Masquelier and P. Simon, *J. Electrochem. Soc.*, 2011, **158**, A1090.

33 V. Augustyn, J. Come, M. A. Lowe, J. W. Kim, P. L. Taberna, S. H. Tolbert and B. Dunn, *Nat. Mater.*, 2013, **12**, 518.

34 X. L. Wu, L. Y. Jiang, F. F. Cao, Y. G. Guo and L. J. Wan, *Adv. Mater.*, 2009, **21**, 2710.